VI International Conference on Adaptive Modeling and Simulation
ADMOS 2013
J. P. Moitinho de Almeida, P. Díez, C. Tiago and N. Parés (Eds)

MATHEMATICAL MODELING OF SPALLATION OF CONDENSED MATTER UNDER THE INFLUENCE OF CONCENTRATED ENERGY FLOW

VLADIMIR I. MAZHUKIN, ALEXANDER V. MAZHUKIN, MIKHAIL M. DEMIN

Keldysh Institute of Applied Mathematics of RAS
Miusskaya sq., 4. Moscow, 125047
e-mail: vim@modhef.ru

Key words: Modeling, Adaptive grid, Dynamic adaptation, Spallation, Laser irradiation.

Abstract. The process of mechanical spallation of a solid aluminum target under the influence of an ultrashort laser pulse is considered. Modeling was carried out using the method of dynamic adaptation with explicit front tracking. The pulse duration was 100 fs, fluence 0.27 J/cm^2. Modeling allowed to determine the thickness of the spalled layers, investigate the regimes in which spallation occurs in melt.

1 INTRODUCTION

The study of dynamic fragmentation in shock loaded metals and evaluation of geometric and kinematic properties of the resulting fragments is a topical issue for both fundamental and applied science. Among the dynamic processes of fragmentation, spall fracture of solid materials has been one of the most widely studied phenomena in a few decades [1,2]. The spallation is defined as a break of the media due to the stress that exceeds the strength of the substance. The main mechanism of rupture is the propagation of a compression pulse in a solid sample, that is reflected from the free surface and after the interaction with the incident unloading wave creates a tensile stress, which can lead to the damage in the material, ranging from small voids and cracks to complete destruction and release of spalled material.

In recent years, there has been increasing interest in such phenomena in the liquid phase, which develop after partial or complete melting, for example, of metals which are exposed at the same time to compression or tension. Rapid heating of the metal target by ultra-short laser pulses (USLP) with femto-and picosecond duration may result in formation of stressed states in the subsurface region. The unloading of these states may result in the ablation of the irradiated melted layer. The process of dynamic fragmentation of liquid leads to the formation of a cloud of liquid droplets ejected into the space at a high speed. Understanding of the physical processes accompanying the process of fast ablation is necessary to determine the optimum regimes of treatment of materials with USLP. The main method of theoretical research is molecular - dynamics simulation [3-5] that uses atomistic models. Continuous models are used much less frequently. Their use is limited by high computational complexity,

which is in the first place associated with the description of the initiation and propagation of the phase fronts.

This paper deals with the theoretical modeling of the mechanisms of fragmentation of liquid, calculation of the process of the ejection of molten droplets and determination of the amount of obtained fragments. The modeling of fragmentation is based on the use of the continuum hydrodynamic non-equilibrium model [6,7].

2 STATEMENT OF THE PROBLEM

Laser radiation propagates from the right to the left and, striking the surface of the metal target, is partly absorbed and partly reflected. The absorbed energy is used for heating, phase changes, generation of shock waves in the solid phase and dynamic fragmentation of the irradiated target. The main features of the high-power laser action on metals are associated with the high speed and volume type of the energy release of the laser pulse in the electronic component. Ultrafast heating of the metal targets by high-power laser pulses causes a strong deviation from the state of local thermodynamic equilibrium (LTE) and requires the appropriate adjustments in the mathematical model. Along with the thermodynamic equilibrium, we should consider the kinetic non-equilibrium of the high-speed phase transitions and strongly overheated metastable states caused by powerful cross-flow of material through the phase boundary. The model should also take into account the powerful dynamic effects associated with the rapid propagation of the phase fronts. The inclusion of these processes requires the explicit description of the kinetics of the phase transitions and the formulation of the conservation laws at the phase fronts, which are hydrodynamic discontinuities. The mathematical description of these processes is accomplished within the framework of the two-temperature and spatially one-dimensional multi-front non-equilibrium hydrodynamic Stefan problem, written for two phases - solid and liquid. When large negative pressure values result in fragmentation of the target, the following mathematical statement is written for both the bulk target and for every spalled part.

2.1 System of equations.

$$\left.\begin{array}{l}
\dfrac{\partial\rho}{\partial t}+\dfrac{\partial(\rho u)}{\partial x}=0\\
\dfrac{\partial(\rho u)}{\partial t}+\dfrac{\partial\left(\rho u^2\right)}{\partial x}+\dfrac{\partial P}{\partial x}=0\\
\dfrac{\partial(\rho_e\varepsilon_e)}{\partial t}+\dfrac{\partial(\rho_e u\varepsilon_e)}{\partial x}=-\left(P_e\dfrac{\partial u}{\partial x}+\dfrac{\partial W_e}{\partial x}+g(T_e)(T_e-T_{ph})+\dfrac{\partial G}{\partial x}\right)\\
\dfrac{\partial\left(\rho\varepsilon_{ph}\right)}{\partial t}+\dfrac{\partial\left(\rho_{ph}u\varepsilon_{ph}\right)}{\partial x}=-\left(P_{ph}\dfrac{\partial u}{\partial x}+\dfrac{\partial W_{ph}}{\partial x}-g(T_e)(T_e-T_{ph})\right)\\
\dfrac{\partial G}{\partial x}+\alpha(T_e)G=0\\
P=P(\rho,T),\quad \varepsilon_e=C_e(T_e)T_e,\quad \varepsilon_{ph}=C_{ph}(T_{ph})T_{ph}
\end{array}\right\}_k ,t>0,\begin{array}{l}0<x<\Gamma_{sl}\cup\\ \Gamma_{sl}<x<\Gamma_{l\upsilon}\end{array} \quad (1)$$

where $W_e = -\lambda_e(T_e, T_{ph})\frac{\partial T_e}{\partial x}, W_{ph} = -\lambda_{ph}(T_{ph})\frac{\partial T_{ph}}{\partial x}, \quad P(\rho, T) = P(\rho_e, T_e) + P(\rho_{ph}, T_{ph}).$

Here: $\rho, u, \varepsilon, T, P$ - are the density, gas-dynamic velocity, internal energy, temperature and pressure of the media respectively, $\alpha(T_e)$ - coefficient of volume absorption, G - density of the laser radiation, $C_{e,ph}$ - heat capacity, $\lambda_{e,ph}$ - heat conductivity, $g(T_e)$ - electron-phonon coupling factor. Indexes s, l, υ correspond to solid, liquid and vapor phases respectively, e, ph - correspond to electron and phonon gas. The expressions for the electron heat capacity, heat conductivity and electron-phonon coupling factor are described in detail in the book [7].

2.2 Initial and boundary conditions

$t = 0: \quad u(0, x) = 0, \quad p = 0, \quad \rho = \rho_0, \quad T_e = T_{ph} = T_0 = 293\,\text{K}.$

On the left stationary border, we write the condition of a zero mass and heat flux:

$x = \Gamma_s: \quad \rho_s u_s = 0, \quad W_T = 0$

On the moving interphase melting boundary $x = \Gamma_{sl}(t)$, we use the boundary conditions according to the non-equilibrium model of melting that is a non-equilibrium kinetic analogue to the equilibrium Stephan problem formulated for a state sufficiently far from the local thermodynamic equilibrium. The system of equations at the boundary consists of the conservation laws of mass, momentum and energy, written for a stationary (laboratory) coordinate system:

$$x = \Gamma_{sl}(t): \quad \rho_s(u_s - \upsilon_{sl}) = \rho_l(u_l - \upsilon_{sl})$$

$$P_{ph,s} + \rho_s(u_s - \upsilon_{sl})^2 = P_{ph,l} + \rho_s(u_s - \upsilon_{sl})^2 \qquad (2)$$

$$\left(\lambda_{ph}\frac{\partial T_{ph}}{\partial x}\right)_s - \left(\lambda_{ph}\frac{\partial T_{ph}}{\partial x}\right)_l = \rho_s L_m^{ne}\upsilon_{sl}$$

These conservation laws are supplemented with the pressure dependence of the melting temperature and kinetic formula for the surface overheating dependence of the melting front velocity $\Delta T_{sl} = T_{sl} - T_m(P_s)$:

$$T_m = T_m(P_s) = T_{m,0} + kP_{ph,s}$$

$$\upsilon_{sl}(\Delta T_{sl}) = \frac{af}{\lambda}(3k_B T_{sl}/m)^{1/2}\left(1 - exp\left(\frac{L_m^{ne}\mu}{R}\frac{\Delta T_{sl}}{T_m T_{sl}}\right)\right)$$

Additional account of the hydrodynamic effects is made by non-equilibrium heat of melting L_m^{ne}:

$$L_m^{ne} = L_m^{eq}(T_m(P_s)) + \Delta C_{ps}\Delta T_{sl} + \frac{\rho_s + \rho_l}{\rho_s - \rho_l}\frac{(u_s - u_l)^2}{2},$$

where $\Delta C_{ps} = (C_{ps} - C_{pl})$.

At the phase boundary, the electronic component is assumed to be continuous relative to the electron density N_e and temperature T_e:

$$\left(\lambda_e \frac{\partial T_e}{\partial x}\right)_s = \left(\lambda_e \frac{\partial T_e}{\partial x}\right)_l,\ T_{e,s} = T_{e,l}.$$

At the moving evaporation front, $x = \Gamma_{kv}(t)$, the model of surface evaporation in the approximation of the Knudsen layer is used as a boundary condition. The model consists of three conservation laws, and three additional parameters at the outer side of the Knudsen layer (T_v, ρ_v, u_v). In general, two of these three parameters are determined using the specific approximating relationships [8], and the third is found from the gas-dynamic equations. The expressions for the evaporation front are given in detail in the book [7].

The boundary conditions for the electron component take the form:

$$-\lambda \frac{\partial T_e}{\partial x} = \sigma T_e^4, \qquad G(t) = (1 - R_k(T_e))G_0 \exp(-(t/\tau_L)^2)$$

where σ - is the Stefan- Boltzmann constant.

At the shock wave in solid, $x = \Gamma_{sh,s}(t)$, we write Rankine-Hugoniot conditions [9] .

3. COMPUTATIONAL ALGORITHM AND METHOD OF DYNAMIC ADAPTATION

The main computational feature of the considered problem is the existence of discontinuous solutions, moving interfacial and contact boundaries. For the numerical solution of the mathematical model (1)-(3), we use the finite-difference method of dynamic adaptation [10]. The method is based on the procedure of transition to an arbitrary nonstationary coordinate system. This transition is made through an automatic conversion of coordinates using the sought solution, which allows formulating the problem of construction and adaptation of the grid at the differential level, i.e. in the resulting mathematical model, one part of differential equations describes the physical processes and the other - the behavior of grid. The method of dynamic adaptation allows to automate the problem of creation of the new domains and perform calculations with explicit tracking of any number of discontinuities, interfacial and contact boundaries. The method of dynamic adaptation and the used finite difference schemes are described in detail in the earlier papers [10-12]. The total number of nodes of the computational grid was set to 200 in the initial target. Additionally, each of the spalled fragments contained approximately 30 nodes in the average.

4. ALGORITHM OF COMPUTATION AND CONSTRUCTION OF COMPUTATIONAL GRIDS

The compression wave, generated due to heating and thermal expansion of the target material, is followed by the rarefaction wave moving from the surface into the interior of the target. If the pressure in the rarefaction wave reaches a sufficiently large negative value, a mechanical spallation may occur, i.e. a formation of voids in the target material. As a result of the spallation, pieces of matter are splitted from the target and move in the direction opposite to the direction of the laser pulse. The spallation is introduced as follows: at the point where the criterion of spallation is met, i.e. at a certain value of the pressure, two new moving boundaries are introduced with saturated vapor between them and boundary conditions describing the kinetics of the surface evaporation and condensation. In the regimes when the temperature in the point of mechanical spallation is not high enough ($T < T_b$), it is possible to replace the saturated vapor with vacuum. That is made for simplicity and without significant loss in accuracy of calculations. Then at these two new boundaries, we use the boundary conditions for the contact discontinuity of condensed matter - vacuum. In addition to the criterion of spallation, we also introduce an additional condition: the minimum size of the spalled material should not be less than several atomic layers, namely 1 nm. A detailed computational grid is automatically generated in the new domain. The nodes of the grid are concentrated on both boundaries according to the law of geometric progression. The minimum spatial step in the spalled domain was set to be 0.01 nm. If the minimum step in moving boundaries was set larger, for example, 0.1 nm, it was not enough to maintain the accuracy in the calculation of the boundary conditions: the amplitude of the periodic oscillations of the gas-dynamic velocity was slowly gradually growing upon reflection from the moving boundaries, while with the sufficient accuracy the amplitude should either not change or decrease due to numerical viscosity. These fluctuations are shown in Fig.7.

When multiple spallations occur, the speed of different spalled parts may be different, and one part may catch up with another. In this case, an algorithm of collapsing of the voids and uniting of two fragments into one was implemented at a certain small distance between the individual phases. This distance was chosen to be 0.4 nm.

The expressions for the spallation criterion were taken from works of Grady [13] and Povarnitsyn [14]. The equation of state used in paper is a modification of EOS from the work of Lomonosov [15].

4.1 Volume melting

The paper of Mei and Lu [16] provides a review of different estimates for the maximum overheating of the solid phase after which volume (homogenous) melting starts. These estimates give the maximum value in the range of 1.1 - 1.38 of the melting temperature. Based on this, we have chosen the following algorithm of consideration of volume melting. When the temperature reaches $1.4T_m$ in some point, $T_m = T_m(p_s)$, then the whole region of solid from the first point where the temperature exceeds T_m is declared to be liquid and the surface melting boundary is moved to that point. The starting temperature of this region is recalculated via the latent heat with the account of the energy conservation law.

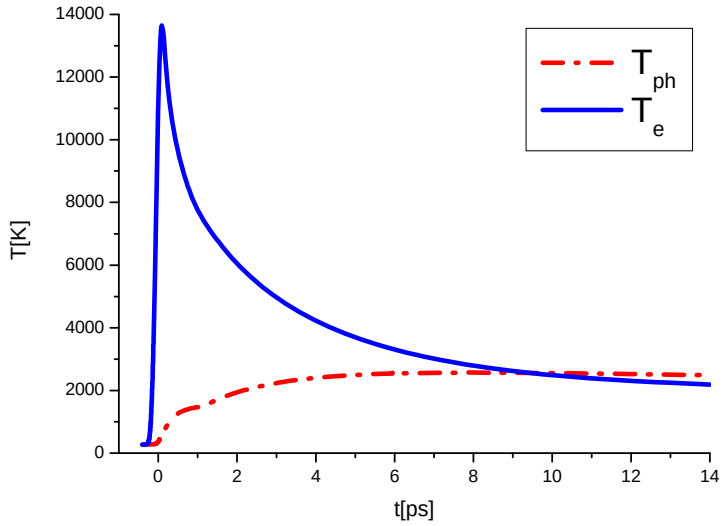

Figure 1. Time dependence of electron and phonon temperature at the target surface.

4. ANALYSIS OF THE RESULTS

Action of USLP on the surface of Al target is considered. The laser pulse with the wavelength $\lambda_L = 0.8\ \mu m$ has Gaussian time profile, $G = G_0 \exp(-(t/\tau)^2)$, with τ =0.1 ps and maximum intensity $G_0 = 1.52 \times 10^{12}$ W/cm^2, corresponding to the fluence $F = 0.27$ J/cm^2. The absorbed fluence is approximately $F_{abs} \approx 0.06$J/cm^2. The computation starts at $t = -4\tau$. Temperature dependence of the surface reflectivity $R(T_e)$ and the volume absorption coefficient $\alpha(T_e)$ were determined through the longitudinal dielectric permeability, which is determined by solving the kinetic equation [17] and with 5% error are approximated by the following analytical expressions:

$R(T_e)$=0.7845465-0.0048568T_e, $\alpha(T_e)$=100exp(13.65497-0.026894T_e+1.66510^{-4}$T_e^{\,2}$).

In these expressions, T_e is measured in electron-volts.

The laser fluence was chosen to be slightly above the spallation threshold, which for our computations was determined to be $F_{th} \approx 0.055$ J/cm^2.

The evolution of the processes in the target is convenient to represent in the form of two consecutive stages: thermodynamically non-equilibrium with $T_e >> T_{ph}$, Fig. 1,2 and hydro-dynamical with $T_e \sim T_{ph}$, Fig. 4–9. Melting of the target starts from the irradiated surface with a large delay relative to the laser pulse, t ~+0.2ps. Significant overheating of the melting surface and high spatial temperature gradients provide high speed of the melting front propagation, υ_{sl} ~2.3km/s, Fig.3. In this paper, the maximum value of overheating of the

solid phase was limited by the value of $1.4T_m$. The decomposition of the overheated metastable state occurs in the form of a volume melting of the overheated region.

The later second stage of the processes $t \geq 0.2$ ps is associated with the evolution of hydrodynamic processes. High speed of the melting front is one of the causes of the appearance of high pressure region in the solid phase, $p_s \sim \rho_s \upsilon_{sl}^2 \approx$ 20kbar, which leads to the formation of the strong compression in front of the melting boundary. Another cause of the compression wave is thermal expansion. Propagation of the compression wave has a loading effect on the substance and corresponds to a positive pressure half-wave. The compression stage is followed by an unloading stage, which corresponds to the negative pressure half-wave.

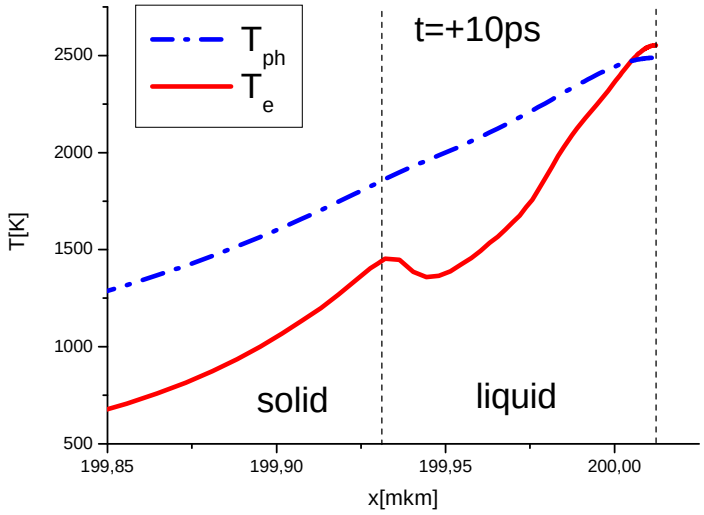

Figure 2. Spatial profile of electron and phonon temperature at t =+10ps.

Fig. 4 shows the pressure profiles before the first spallation and right after that. Fig. 5 and 6 show the density profiles and electron and phonon temperatures at t =+0.4 ns. There are 9 spalled parts seen at the figures with sizes from 2 to 19 nm. There were 20 spallation events in this computation, some of the spalled parts joined and formed larger fragments. The total size of the spalled material, converting via the density of solid, is 78 nm which is in good agreement with the values reported from MD simulation [18]. The temperature of the spalled parts is in the range from 1000K to 2100K. Repeated passage of the pressure waves, reflected from the left and right free boundaries, is observed in each of the spalled parts. These waves are most noticeable in the parts with the maximum sizes, in this modeling these are the most left and most right part with the sizes 45 nm and 35 nm correspondingly, where the pressure amplitude reaches the value of 1-2GPa. Fig. 7 shows the time dependence of hydro-dynamic velocity (black curve) at the right free boundary of the target (bulk liquid or solid), at the left boundary of the most left spalled part (red curve), the closest to the bulk target, and at the right boundary of the most right fragment, the farthest from the bulk target. The frequency of the velocity oscillations is different in different parts due to the different sizes of the parts.

Also, there are several velocity peaks during one period. That is caused by the fact that these fragments were created as a result of collision of several smaller parts which already had own oscillations with own frequency. The average movement velocity is about 200m/s for the left part and 500 m/s for the right part. It should be noted that in this modeling, almost entire liquid is spalled after the passage of the rarefaction wave, and the remaining 6 nm of liquid are already crystallized at the moment +0.4ns. Figure 7 shows the amount of liquid in bulk and in the spalled parts. It is seen that the whole liquid is spalled except the mentioned 6 nm. Figure 3 shows the velocity of the melting front. The maximum value of velocity reaches the value of 2300 m/s. At the moment +45ps, melting ceases completely and crystallization starts. The maximum crystallization velocity is 58 m/s.

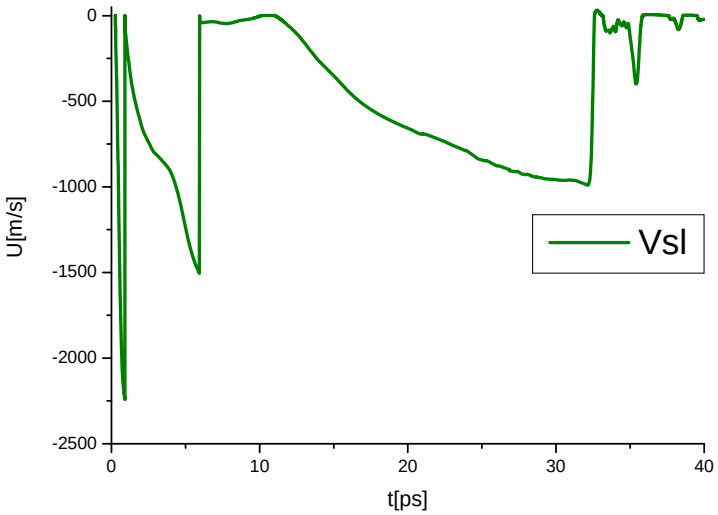

Figure 3. Melting front velocity.

5. CONCLUSION

Algorithm of solution of the problem of laser ablation in a multiply-connected domain area using the dynamic adaptation method was developed. This algorithm was used to investigate the mechanism of fragmentation of a massive metal target by ultrashort laser pulses. A good agreement with molecular dynamic simulation for the spallation threshold and the amount of the fragmented material is obtained.

ACKNOWLEDGMENT

This study was partly supported by RFBR grants 13-07-00597-a, 12-07-00436-a.

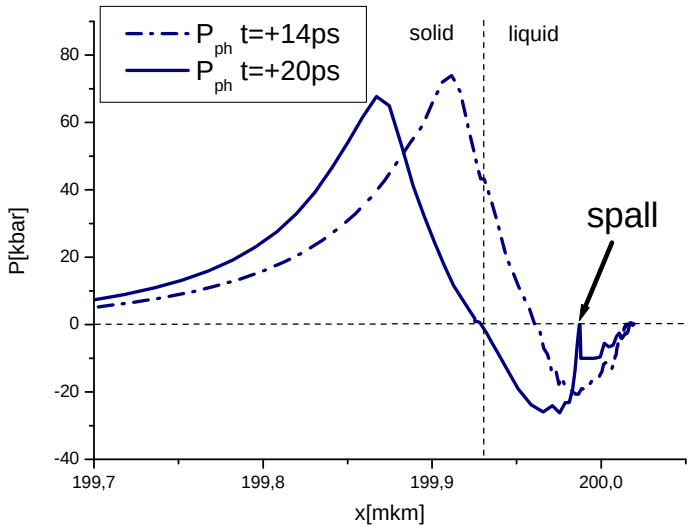

Figure 4. Pressure profiles before and after first spallation.

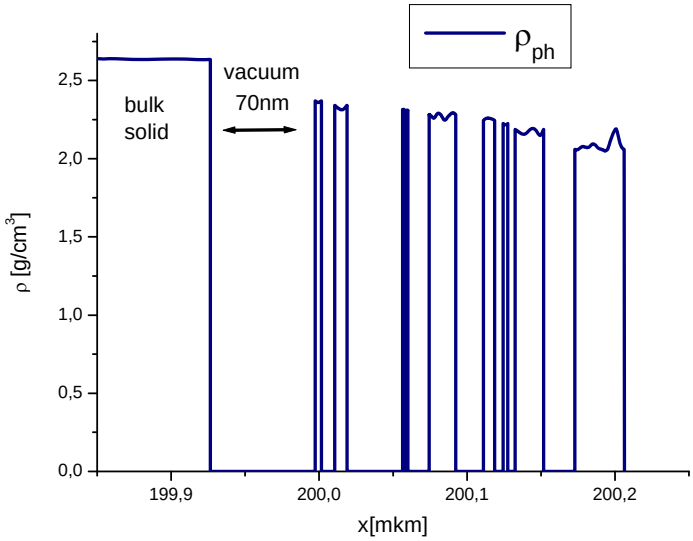

Figure 5. Density profile at t= +0.4ns

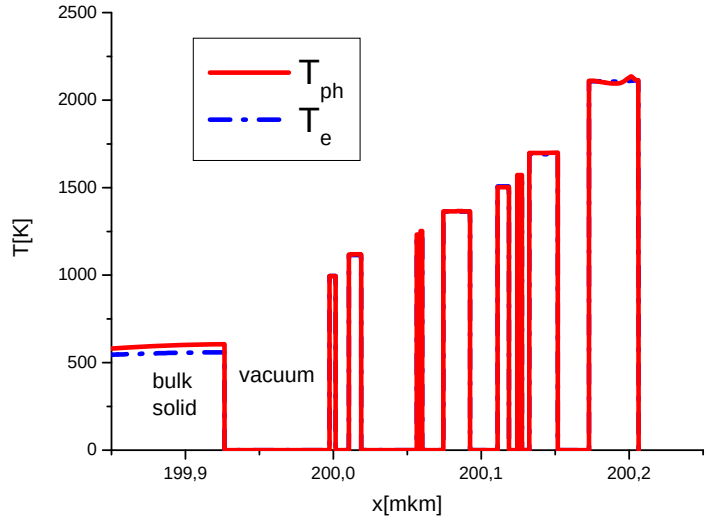

Figure 6. Electron and phonon temperature at t= +0.4ns

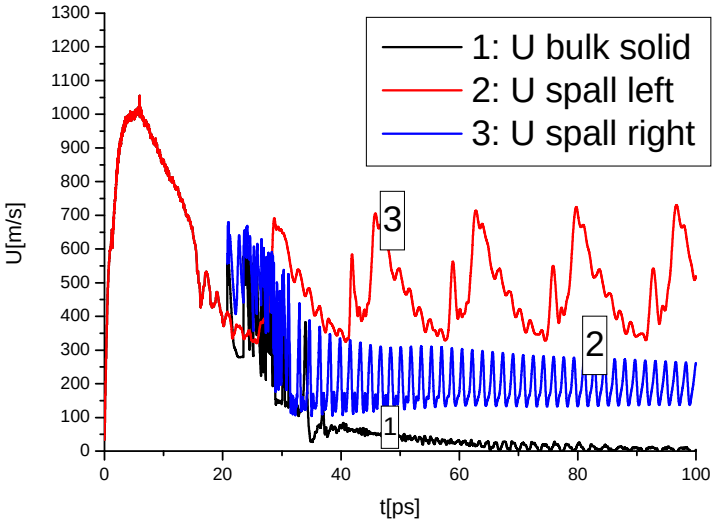

Figure 7. Hydro-dynamic velocity at the very right boundary of bulk phase, right boundary of the right spalled part and left boundary of the left spalled part.

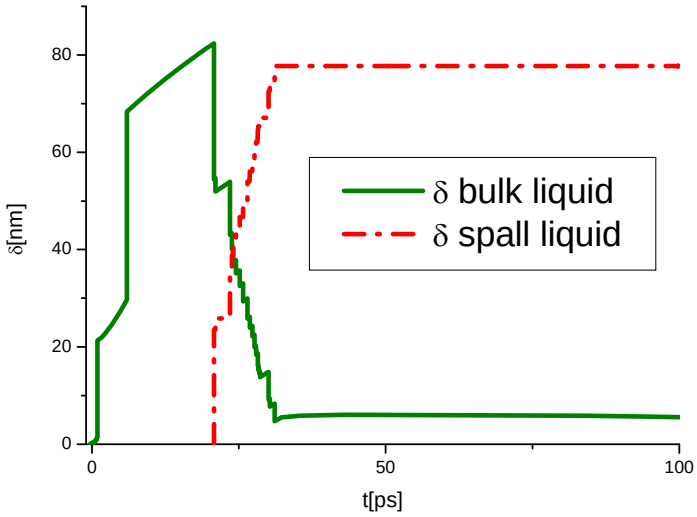

Figure 8. Amount of material in bulk liquid and spalled liquid.

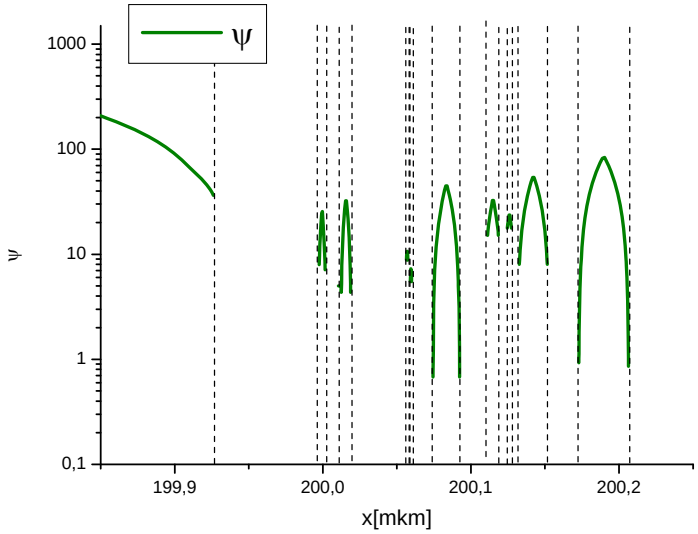

Figure 9. Non-dimensional grid step.

REFERENCES

[1] Davison, L., Grady, D. E. and Shahinpoor, M. *High Pressure Shock Compression of Solids II: Dynamic Fracture and Fragmentation.* Springer, New York, 1996.

[2] Antoun, T., Seaman, L., Curran, D. R., Kanel, G. I., Razorenov, S. V. and Utkin, A. V. *Spall Fracture.* Springer, Berlin, 2002.

[3] Ivanov, D. S. and Zhigilei, L. V. Combined atomistic-continuum modeling of short-pulse laser melting and disintegration of metal films. *Phys. Rev. B* (2003) **68**:064114

[4] Perez, D. and Lewis, L. J. Molecular-dynamics study of ablation of solids under femtosecond laser pulses. *Phys. Rev. B* (2003) **67**: 184102

[5] Stegailov, V. V., Starikov, S. V. and Norman, G. E. Atomistic simulation of laser ablation of gold: The effect of electronic pressure. *AIP Conf. Proc*. (2012) **1426**: 905;

[6] Mazhukin, V.I., Mazhukin, A.V., Demin, M.M. and Shapranov, A.V. - Mathematical modeling of short and ultrashort laser action on metals. *Surface Modification Technologies (SMT 24)*. Eds. T.S.Sudarshan, Eckhard Beyer, Lutz-Michael Berger, (2011), **24**: 201-208. (ISBN 978-81-910571-2-6).

[7] Mazhukin, V.I. Kinetics and Dynamics of Phase Transformations in Metals under action of ultra-short high-power laser pulses. Ch. 8, pp.219 - 276. In "*Laser Pulses – Theory, Technology, and Applications"*, Ed. by I. Peshko. 2012, P. 544, InTech, Croatia.

[8] Mazhukin, V.I. and Samokhin, A.A. Boundary conditions for gas-dynamical modeling of evaporation processes. *Mathematica Montisnigri*, 2012, vol. XXIV, pp.8 - 17.

[9] Landau L. D., Lifshic E. M. Teoreticheskaja fizika, t. V. Statisticheskaja fizika. Chast' 1. (1976) M.: Nauka. 616 p.

[10] Mazhukin, A.V., Mazhukin, V.I. and Breslavskii, P.V. Dynamic adaptation in gas dynamics problems with non-linear heat conductivity. *Proceedings of the V International Conference on Adaptive Modeling and Simulation (ADMOS 2011)*, Eds. D.Aurby, P.Diez, N.Pares. Paris, France. (2011) 105 - 116.

[11] Mazhukin, V.I., Mazhukin, A.V. and Shapranov, A.V. Dynamic adaptation in differential equations of the parabolic type in partial derivatives. *Encyclopedia of low-temperature plasma*, Series B, Vol. VII –1, Mathematical modeling in low-temperature plasma, Part 1, pp. 190 – 216, Moskva, Yanus-K (2008).

[12] Mazhukin, V.I., Mazhukin, A.V. and Shapranov, A.V. Dynamic adaptation in differential equations of the hyperbolic type in partial derivatives. *Encyclopedia of low-temperature plasma*, Series B, Vol. VII –1, Mathematical modeling in low-temperature plasma, Part 1, pp. 217 - 247, Moskva, Yanus-K (2008).

[13] Povarnitsyn, M. E., Itina, T. E., Sentis, M., Khishchenko, K. V. and Levashov P. R. Material decomposition mechanisms in femtosecond laser interactions with metals (2007) Phys. Rev. B. **75**:235414.

[14] Grady, D. E. The spall strength of condensed matter. *J. Mech. Phys. Solids* (1988) **36**: 353-384.

[15] Lomonosov, I.V. Multi-phase equation of state for aluminum. *Laser and Particle Beams* (2007) **25**:567–584.

[16] Mei, Q.S. and Lu, K. Melting and superheating of crystalline solids: From bulk to nanocrystals. *Progress in Materials Science* (2007) **52**:1175–1262.

[17] Mazhukin V.I., Mazhukin A.V., Koroleva O.N. Optical properties of electron Fermi-gas of metals at arbitrary temperature and frequency. *Laser Physics*, (2009) **19**:1179-1186.

[18] Zhakhovskii, V, Inogamov, N and Nishihara, K. Laser ablation and spallation of crystalline aluminum simulated by Molecular Dynamics. *Journal of Physics: Conference Series* (2008) **112**:042080